ABSTRACT

Title of Thesis: THE EFFECT OF ZINC IN CARBON CONCENTRATING MECHANISMS IN *PHAEODACTYLUM TRICORNUTUM*

Nairui Zhou, Master of Science, 2015

Thesis Directed By: Dr. Ganesh Sriram
Department of Chemical and Biomolecular Engineering

Photosynthesis is crucial for life but is a slow process because the CO_2 concentration near the principal carbon-assimilation enzyme RuBisCO is extremely low. Very few plants and algae perform a carbon-concentrating mechanism (CCM) to overcome the insufficiency, which are classified into biophysical and biochemical (C_4) mechanism. The enzyme CA catalyzes the reversible dehydration of HCO_3^- to CO_2 in biophysical CCMs and its active site contains a Zn^{2+}. In this study, we hypothesized that Zn^{2+} availability can impact CCMs and therefore investigated the effect of Zn^{2+} availability on photosynthetic metabolism in a unicellular marine diatom *Phaeodactylum tricornutum*. *P. tricornutum* has a sequenced genome and can conduct both biophysical and C_4 CCMs. We observed that Zn^{2+} has a significant effect on cell growth rate but no significant interference on intracellular metabolism, suggesting no essential compensation of C_4 CCMs for biophysical CCMs even at low CA activity anticipated at low Zn^{2+} concentration.

THE EFFECT OF ZINC IN CARBON CONCENTRATING MECHANISMS IN *PHAEODACTYLUM TRICORNUTUM*

by

Nairui Zhou

Thesis submitted to the Faculty of the Graduate School of the
University of Maryland, College Park, in partial fulfillment
of the requirements for the degree of
Master of Science
2015

Advisory Committee:
Dr. Ganesh Sriram, Chair
Dr. Amy J. Karlsson
Dr. Jeffery B. Klauda

Acknowledgements

This study was designed with the help of Dr. Ganesh Sriram and Andrew Quinn, experiments and analysis were conducted with the assistance of Andrew Quinn. Dr. Sriram critically reviewed the draft manuscript. This study was supported by National Science Foundation (grant number: CBET-1134115).

Table of Contents

List of Tables

List of Figures

List of Abbreviations

3PG	3-phosphoglyceric acid or glycerate-3-phosphate
αKG	α-ketoglutarate
Ala	alanine
Asp	aspartic acid
CA	carbonic anhydrase
CCM	carbon concentration mechanism
DMF	dimethylformamide
DI	deionized
GC-MS	gas chromatography-mass spectrometry
Glu	glutamic acid
Gly	glycine
ILEs	isotope labeling experiments
Mal	malate
MDH	Mal dehydrogenase
ME	malic enzyme
MID	mass isotopomer distribution
MTBSTFA	N-(tert-butyldimethylsilyl)-N-methyltrifluoroacetamide
OAA	oxaloacetate
ODE	ordinary differential equation
PEP	phosphoenolpyruvic acid or phosphoenolpyruvate
PEPC	phosphoenolpyruvate carboxylase
Phe	phenylalanine
Pyr	pyruvic acid or pyruvate
P. tricornutum	*Phaeodactylum tricornutum*
RuBisCO	ribulose 1, 5-bisphosphate carboxylase/oxygenase
SIM	selected ion monitoring
SD	standard deviation
Ser	serine

SVD	singular value decomposition
TBDMCS	tert-butyldimethylchlorosilane
TM	trace metal
Tyr	tyrosine
UV-Vis	ultraviolet–visible
Val	valine

Chapter 1: Introduction

1.1. Photosynthesis and CO_2

Photosynthesis is a process performed by plants, algae and cyanobacteria to convert light energy into chemical energy, atmospheric CO_2 to reduced carbon and water to oxygen. Thus, photosynthesis fuels the activities of heterotrophic organisms and is indispensable for life on earth. Despite this, photosynthesis is slow in most plants because the CO_2 concentration around the principal carbon-assimilation enzyme, ribulose-1,5-bisphosphate carboxylase/oxygenase (RuBisCO), is quite low (atmospheric CO_2 concentration ~400 ppm) (Ellis, 2010; Haimovich-Dayan et al., 2013). RuBisCO can only utilize CO_2 instead of HCO_3^- or CO_3^{2-}, and CO_2 is sparingly soluble in water with an aqueous molecular CO_2 concentration of ~13 μM.

The concentration is much lower than the $K_{1/2}(CO_2)$ of RuBisCO (20-40 μM) (Badger et al., 1998), which results in a much slower reaction rate than the maximal one. There is also evidence showing that O_2 can worsen the situation further by acting as a competitive inhibitor of RuBisCO (Wingler, 2000). This inhibition, which is favorable over 30 °C, results in a process called photorespiration that is energy and oxygen consuming to protect the cells from high light conditions by dissipation of light energy (Parker & Armbrust, 2005). This pathway fixes oxygen with the same enzyme and substrate as CO_2 fixation, approximately 25% of reaction on RuBisCO produces a product that cannot be used within the Calvin–Benson cycle, resulting a hold back in fixation (Parker, Armbrust, Piovia-Scott, & Keil, 2004).

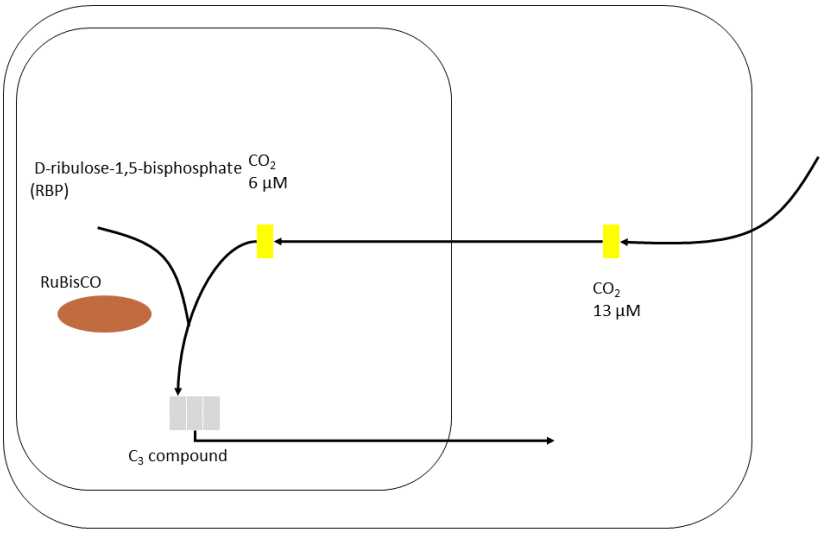

Figure 1 Photosynthetic environment inside cells.
Large rounded rectangle: cell, small rounded rectangle: chloroplast,
yellow marker: molecular CO_2, brown oval: RuBisCO, gray markers: C_3 compound.
Molecular CO_2 comes into the cells and the chloroplast, and is converted into
C_3 compound.

1.2. CCM in algae

Oceans cover 70% of the Earth, and the marine algae living in the water do not need to face the problem of decreasing cultivated land, making marine algae an attractive research focus with potential for carbon fixation and ultimately biofuel production. Utilization of marine algae could alleviate the burden of limited cultivated land that is still reducing, as well as avoiding the problem of competing with food (Doan, Sivaloganathan, & Obbard, 2011). As is mentioned above, CO_2 is slightly soluble in water under ambient conditions (~13 µM, even lower ~6 µM near RuBisCO), posing a hindrance to efficient photosynthesis (Fig. 1). It is, therefore, fascinating that marine algae are successful and playing an important role in fixing the CO_2 despite such a severe condition. They could live in the water while the ambient concentrate of CO_2

is very insufficient, indicating that carbon-concentrating mechanisms (CCMs) exist in them (Raven, 2010; Roberts, Granum, Leegood, & Raven, 2007b) to overcome potential limitations of an inefficient RuBisCO activity and prompt the photosynthesis rates. The CCMs is valuable for its function in enhancing the efficiency of photosynthesis with limiting CO_2 and can be great asset if it is applicable to other land plants. However, details about the operation of CCMs are not explicitly known, so the investigation on CCMs becomes essential for solving the tardiness of photosynthesis. There are two hypotheses about the process of CCM (Reinfelder, 2011; Roberts, Granum, Leegood, & Raven, 2007a): biophysical and biochemical C_4 mechanisms, both of them could use HCO_3^- directly, the dominant form of inorganic carbon dissolved in water. The growing demand of carbon consumption calls for research on enhancing the efficiency of photosynthetic output, and CCMs can be regarded as a powerful pathway.

In water, especially in the high salinity and slightly alkaline pH (~8) of the ocean, CO_2 dissociates and the equilibrium favors the formation of bicarbonate (HCO_3^-) (Reinfelder, 2011). The biophysical mechanism could convert the reversible hydration of HCO_3^- to CO_2 with the assistance of ubiquitous enzyme carbonic anhydrase (CA, EC 4.2.1.1):

$$CO_2 + H_2O \rightleftharpoons H^+ + HCO_3^-,$$

so that the CO_2 concentration in vicinity of RuBisCO will be remarkably enhanced either at surface of the algae cell or at the site of carbon fixation by RuBisCO in the

cell's chloroplast (Fig. 2). CA activity has been measured in many other algal species including diatoms (Reinfelder, 2011), but the specific role of CA is still elusive.

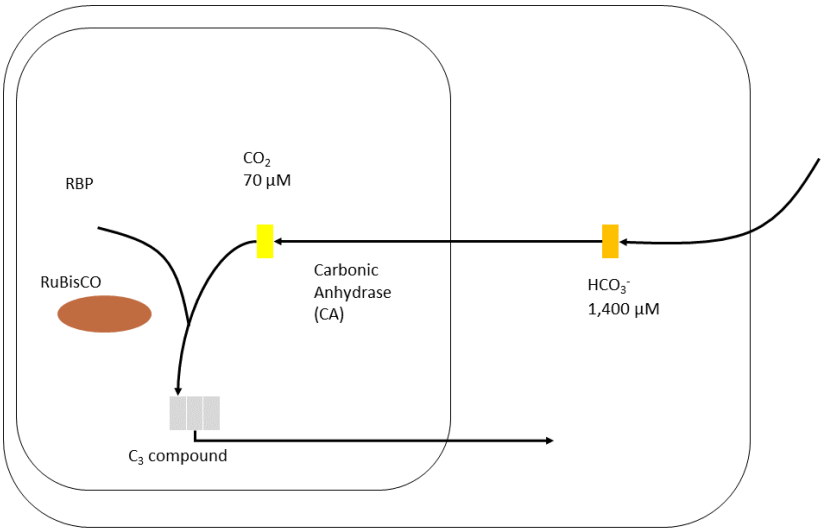

Figure 2 Hypothesized biophysical CCMs in diatoms.
Large rounded rectangle: cell, small rounded rectangle: chloroplast,
yellow marker: molecular CO_2, orange marker: HCO_3^-, brown oval: RuBisCO,
gray marker: C_3 compound.
HCO_3^- comes into the cell and converts to molecular CO_2 that can be utilized by RuBisCO and accumulates either inside or outside the chloroplast with the catalysis of CA. CO_2 then goes through photosynthesis pathway and is converted into C_3 compound which is shown in gray marker.

There is a Zn-C co-limitation that is proposed since CA is a metalloenzyme which has Zn, Co and/or Cd as cofactors (Morel et al., 1994; Xu, Feng, Jeffrey, Shi, & Morel, 2008). The activity of maintaining equilibrium between HCO_3^- and CO_2 may not be able to provide the desirable CO_2 concentration without high HCO_3^- near the CA and RuBisCO (Badger & Price, 1994; Bowler et al., 2008). There are two types of biophysical CCMs reported. In one type, the HCO_3^- is converted to CO_2 by CA catalysis outside the cell or compartment surface and is transported through the

membranes by passive diffusion. In the other one, HCO_3^- enters the cell or compartment directly and is converted by internal CA near the RuBisCO(Reinfelder, 2011).

The biochemical mechanism, also is addressed as C_4 mechanism, does not utilize HCO_3^- directly. Instead, this mechanism uses “anaplerotic” (biomass-synthesizing) enzymes to condense HCO_3^- with a C_3 compound such as phosphoenolpyruvate (PEP) or pyruvate , resulting in a C_4 compound such as oxaloacetate (OAA) and malate (Mal) (Rech, Morant-Manceau, & Tremblin, 2008). Generally speaking, the C_4 metabolism relies on two steps (Fig. 2). HCO_3^- first undergoes carboxylation using phosphoenolpyruvate carboxylase (PEPC), which usually happens in mesophyll cells, then the C_4 compound is transported into bundle sheath cells (Reinfelder, Kraepiel, & Morel, 2000; Reinfelder, Milligan, & Morel, 2004). In bundle sheath cells, the CO_2 is released through decarboxylation and therefore CO_2 concentration in close range of RuBisCO is enhanced. The spatially separated mechanisms usually call for multiple cell types, however, the two steps are also reported to happen in a single cell in different subcellular compartment.

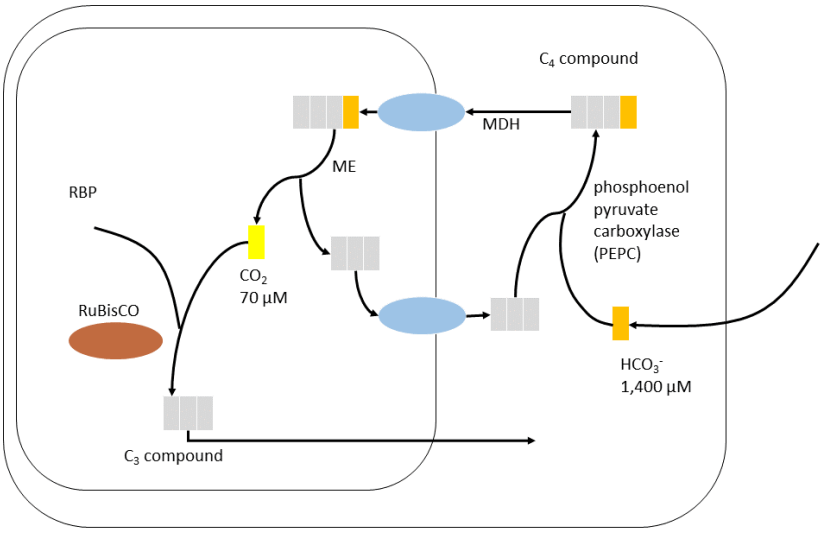

Figure 3 Hypothesized biochemical CCMs in diatoms.
Large rounded rectangle: cell, small rounded rectangle: chloroplast,
yellow marker: molecular CO_2, orange marker: HCO_3^-, gray markers: C_3 compounds,
markers with gray and orange color: C_4 compounds.
Blue oval markers: proteins participate in the active transport of C_4 compounds,
brown oval: RuBisCO.

HCO_3^- comes into the cell and converted into C_4 compound combined with a C_3 compound under the catalysis of enzymes such as PEPC. C_4 is then transported with the assistance of proteins into the chloroplast where it is decomposed into C_3 compound and molecular CO_2. C_3 compound is transported out of chloroplast to combine an HCO_3^- again, forming a C_4 cycle. Molecular inside the chloroplast is utilized by RuBisCO and participates the photosynthesis pathway.

1.3. CCM in diatoms

Diatoms are a major group of algae and are one of the most common type of algae. Diatoms are unicellular even though they can form colonies in different shapes, and

they possess a unique cell wall made of SiO_2 which is called frustule with yellowish-brown chloroplast enclosed. It is estimated that more than 200 genera and 100,000 extant species of living diatoms, contributing up to 45% of the total oceanic primary production and 20% of total global primary production (Falkowski & Raven, 2013); and also diatoms are responsible for more than 50% of organic carbon flux to the deep ocean (Dugdale & Wilkerson, 1998; Reinfelder, 2011). Spatial distribution of diatom is wide both in ocean and in fresh water, with remarkably differences in nutrient uptake, photoacclimation, and growth. Inorganic carbon acquisition strategies also vary among diatom species due to the diversity (Goldman, McGillicuddy Jr, & others, 2003; Marchetti, Maldonado, Lane, & Harrison, 2006).

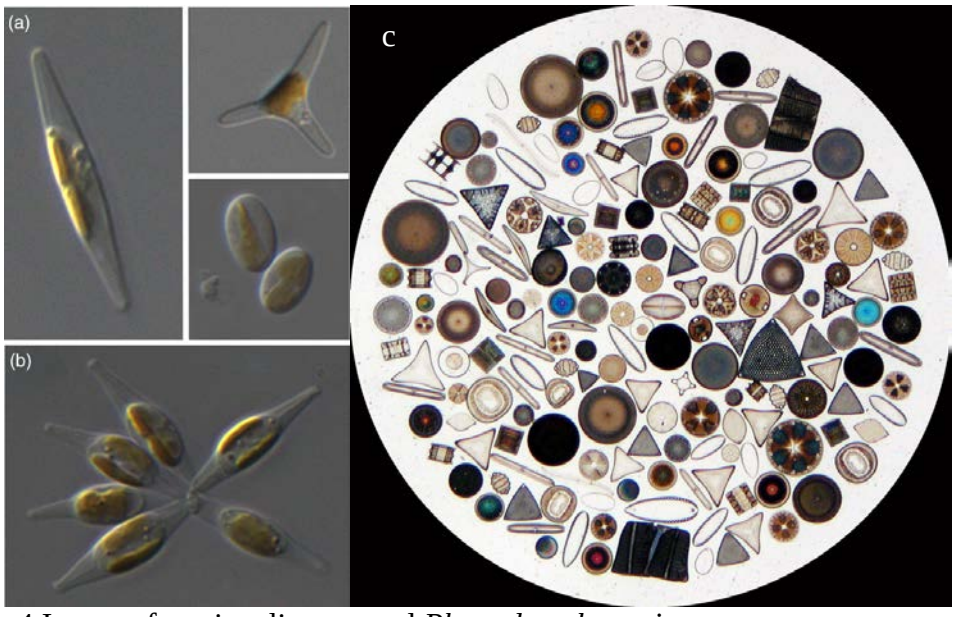

Figure 4 Image of marine diatoms and *Phaeodactylum tricornutum*
(a) *Phaeodactylum tricornutum* (Vardi, Thamatrakoln, Bidle, & Falkowski, 2008). Left: fusiform, top right: triradiate, bottom right: oval. Image by A. D. Martino. (b) A cluster of *P. tricornutum*. (c) Diatom ("Diatom," 2015).

As mentioned above, the ability of CA maintaining equilibrium between two forms of CO_2 alone would not be able to obtain high CO_2 concentration near RuBisCO,

investigation has been done to the upregulation and a carbon pump was proposed (Morel et al., 1994; Roberts et al., 2007a). Marine diatoms express adequate enzymes that are necessary for a photorespiratory pathway for RuBisCO to consume waste O_2 that competes with CO_2 and can hold back carbon fixation, but even at insufficient CO_2 environment, the photorespiratory reaction maintains at a low level, which is a strong pointer that diatoms possess an active carbon pump along with CA to maintain a high concentration of CO_2 near RuBisCO (Parker & Armbrust, 2005; Rech et al., 2008).

Experiments have shown that activity of CA is inversely related to the CO_2 concentration in medium, but extracellular CA activity is low and not always related to CO_2 (Morel et al., 1994). Even though the assistance of inorganic carbon uptake still depends the intracellular location of CA: a putative model of cytoplasmic CA could hydrate the CO_2 transported into the cell to HCO_3^- so that HCO_3^- can be trapped and stored in the cytoplasm, therefore in general both forms of inorganic carbon come into the cell through active transport; the chloroplast CA would simply provide direct supply of CO_2 to RuBisCO through dehydration of HCO_3^- (Reinfelder, 2011).

1.4. Phaeodactylum tricornutum

Phaeodactylum tricornutum is a unicellular pennate marine diatom in the genus *Phaeodactylum*. *P. tricornutum* has multiple morphotypes (fusiform, triradiate, and oval) (Fig. 4b) , and the morphotypes can be stimulated by environmental conditions (Borowitzka & Volcani, 1978). Although being a diatom, *P. tricornutum* can survive in environments without silica and in the absence of frustule, which is unlike most of

the diatoms. There is another character is that the frustule does not decrease during asexual reproduction, therefore continuous subculture can be conducted without demand of sexual reproduction (Lewin, Lewin, & Philpott, 1958), making *P. tricornutum* suitable for many experimental researches.

P. tricornutum could be an excellent experimental subject for investigation of CCMs in single cells since its genome has been sequenced (Bowler et al., 2008; Kroth et al., 2008) and there are reports demonstrating genetic toolkits available. It is assumed that *P. tricornutum* is able to operate CCMs; however, the specific pathway of CCMs in it remained elusive for quite a spell. Although some diverse opinion exists, there is evidence for biophysical and biochemical CCMs existing in *P. tricornutum*, both circumstantial and direct. Also, genome bioinformatic analyses indicated that *P. tricornutum* is one of the only two species of algae that can perform operate both a biophysical and a biochemical CCMs (Badger & Price, 1994; Harada & Matsuda, 2005; Kroth et al., 2008).

As evidence of biophysical CCMs, two of the nine putative CAs can be traced in *P. tricornutum* (Kitao, Harada, & Matsuda, 2008), and there are data showing CA activity in concentrating CO_2 using isotope labeling experiments (ILEs). And also research on expressing genes encoding putative C_4 CCMs enzyme under different circumstances were reported, supporting the view of C_4 CCMs (Reinfelder et al., 2004).

1.5. Carbonic anhydrase

Carbonic anhydrase (CA) (or carbonate dehydratases) is an important family of enzymes that can catalyze the reversible reaction between two forms of inorganic carbon, that is, hydration of CO_2 and dehydration of HCO_3^-. Most CAs contain a Zn^{2+} in their active site, therefore they are classified as metalloenzymes. CA exists widely in many different species including mammals, plants and algae, and has one of the fastest catalytic reaction rate that is mostly limited by the diffusion of its substrate. CA has at least six various families (α, β, γ, δ, ζ and η), and most prokaryotic and plant chloroplast CAs belong to the beta family (β-CA) (Badger & Price, 1994; Reinfelder, 2011).

It was generally accepted that intracellular carbonic anhydrase activity was essential for CCMs since the treatment of *P. tricornutum* cells with ethoxyzolamide, which is a highly permeable CA inhibitor has abolished high affinity photosynthetic pathway while acetazolamide, a weakly permeable CA inhibitor, turned out ineffective (Harada & Matsuda, 2005). Also investigation shows that CA activity is inversely related to the inorganic carbon concentration in acclimation media as the only carbon source. Hence conclusion can be drawn that CA activity would directly or indirectly adjust the carbon fixation, photosynthesis rate and further cell growth and reproduction. Since CA calls for Zn^{2+} on its active site in structure, we assume that a low Zn^{2+} concentration may inhibit the activity of CA; further inhibit the biophysical mechanism and efficiency of photosynthesis, with changes in metabolic fluxes as well.

There is evidence showing that in a Zn deficient marine environment, Co and Cd can substitute in the active site of CA (Lane & Morel, 2000; Yee & Morel, 1996), or a distinct CA from ζ family that uses a cadmium cofactor can be utilized (Lane et al., 2005; Lane & Morel, 2000); therefore, Co and Cd are also needed to be constrained in the investigation while down-regulating the Zn^{2+} concentration. In the research, we intended to adjust the Co^{2+} and Cd^{2+} concentrations as well as Zn^{2+}; however, L1 medium recipe (National Center for Marine Algae and Microbiota, NCMA) does not include cadmium in its trace element solution, which prevent us from setting cadmium concentration as a variable in the investigation.

Table 1 Natural abundance and L1 concentration of Zn^{2+}, Co^{2+} and Cd^{2+}.
Natural abundances are metal ion concentrations in sea water, abundance in L1 recipe are the concentration in final L1 medium that is ready for culturing.

Metal ion	Natural abundance	L1 recipe
Zn^{2+}	5.13×10^{-9} M	8.00×10^{-8} M
Co^{2+}	2.05×10^{-11} M	5.00×10^{-9} M
Cd^{2+}	6.15×10^{-10} M	0 M

Note. Concentration are given by L1 medium recipe from NCMA, calculated from trace element stock solution.

In this work, we investigated the effect of Zn^{2+} concentration on CCMs. We performed ordinary incubation as well as isotope-labeling experiments (ILEs) by feeding ^{13}C bicarbonate as carbon source. Then, gas chromatography-mass spectrometry (GC-MS) was introduced to measure the metabolite pattern under various circumstances at different time ranges, and we analyzed selected ILEs by application of MATLAB programs and analyzing the MID data. These experiments and analyses turned out partially confirming our hypothesis.

Chapter 2: Materials and Methods

2.1. Modified L1 Medium and cell culture

The L1 medium recipe was modified in order to investigate the effect of Zn^{2+}. Modification was made merely to trace element component, with various Zn^{2+} concentration levels. Concentration details are given in the Table. 2. All elements that are not mentioned in Table. 2 remained the same level throughout the experiment as provided by L1 recipe. To eliminate the effect of Co^{2+}, we set Condition 1 with no additional Zn^{2+} and Co^{2+} brought in the medium by trace element solutions. Since there is no Cd^{2+} concentration mentioned in the L1 recipe, we did not set up concentration gradient for Cd^{2+}; therefore all five conditions share a same level of Cd^{2+} consistent of marine water. Investigation on increasing the Cd^{2+} concentration could be performed in future study; however, reducing the Cd^{2+} concentration would be difficult to perform.

The marine diatom *P. tricornutum* (strain PEPC. b) was obtained from the NCMA (East Boothbay, ME), and was maintained aseptically. The cell culturing was grown in 125 mL Erlenmeyer flasks with 50 mL modified L1 culture medium, four bio-replicates of each condition. The flasks were placed in refrigerated New Brunswick Innova 44R shakers (Eppendorf Hauppauge, NY), with programmed temperature at 24.5 °C and constant light.

Table 2 Zn^{2+} and Co^{2+} level in modified L1 medium.
Condition 1 to Condition 5 formed a concentration gradient of Zn^{2+}, while Condition 3 can be considered as original L1 medium and control group. Groups of cultures under different conditions would be addressed as Condition 1 to 5. Media were made using same stock solutions.

Condition	Zn^{2+} Concentration	Co^{2+} Concentration
#1	5.13×10^{-9} M	2.05×10^{-11} M
#2	5.13×10^{-9} M	5.00×10^{-8} M
#3	1.31×10^{-8} M	5.00×10^{-8} M
#4	8.51×10^{-8} M	5.00×10^{-8} M
#5	1.72×10^{-7} M	5.00×10^{-8} M

P. tricornutum cells were incubated for two weeks after subculture, and cell counting was performed on DHC-N01 hemocytometers (INCYTO, Chungnam, Korea) throughout the period to monitor the growth.

2.2. Instationary Isotope Labeling Experiment (ILE), cell harvest, metabolite extraction and derivatization

To further investigate the effect of Zn^{2+} concentration on metabolism, isotope labeling experiments were conducted with Condition 1, Condition 3 and Condition 5 cells. Cells were subcultured from previous cell growth research each with corresponding Zn^{2+} level, while other conditions remained the same.

2.2.1. Short time instationary ILE

In order to obtain obvious difference in growth, cells were cultured in modified L1 medium for 12 days before next treatments. Cell suspensions were first transferred from flasks to 50 ml centrifuge tubes and then were centrifuged at 8000 min^{-1} for

5 min. Next most of the supernatant (medium) was removed and the cells were left with ~1 mL of medium. The cells were mixed by slightly shaking and transferred to 2 mL pre-sterilized micro-centrifuge tubes and centrifuged at 13300 min^{-1} at -4 °C for 1 min, after that the supernatant was removed again. 0.5 mL of modified L1 medium containing 25 g L^{-1} $NaH^{13}CO_3$ was added into each micro-centrifuge tube, and the cell pallets were resuspended by shaking quickly. Three biological replicates were represented of each condition at three different time points (1min, 5 min, and 30 min). Tubes were immediately immersed into liquid nitrogen at appropriate time points to quench metabolism.

2.2.2. Long time instationary ILE

Longer instationary ILEs were performed in triplicate in shake flasks and no pre-processing was needed. 0.5 ml of modified L1 medium containing 25 g L^{-1} $NaH^{13}CO_3$ was added into the flasks directly, and the experiments lasted for time range of 240 min (4 h) and 480 min (8 h). To harvest at the end of experiment, cell suspensions were centrifuged at 8000 min^{-1} for 5 min and most of the medium was removed. The cells were slightly shaken and mixed before transferred into 2 ml micro-centrifuge tubes. After that the tubes were centrifuged at 13300 min^{-1} at -4 °C for 30 s, most of the supernatant was removed again and the tubes were quenched in liquid nitrogen.

^{12}C experiments were conducted at the same time where cells were cultured separately for 12 days with unlabeled carbon source in modified L1 medium in three replicates of each condition. Unlabeled cells were harvested as well in order to

quantify metabolite pool sizes (concentrations), after which same procedure of metabolite extraction, derivatization and quantification were performed.

2.3. Intracellular metabolite extraction and derivatization

After tubes were quenched in liquid nitrogen, 0.7 mL boiling methanol and 25 µL deionized H_2O were added into the tubes to isolate intracellular metabolites to break the cell walls, tubes were then incubated at 30 °C to 35 °C for 30 min. Then 0.7 mL deionized H_2O and 0.37 mL chloroform were added when the liquid in the tubes turned green to separate polar and non-polar layers. The tubes were briefly vortexed and then centrifuged at 13,300 min^{-1} at -4 °C for 10 min. The upper layer (methanol/H_2O) was collected and evaporated overnight under ambient condition. The obtained sample was mixed with 80 µL deionized H_2O and 20 µL solution of of 10 mg mL^{-1} norleucine as internal standard, transferred into a 350 µL GC vial and lyophilized overnight.

50 µL solution of 20 mg mL^{-1} methoxyamine hydrochloride in pyridine was added into the lyophilized mixture for reconstitution, the reaction was kept at 30 °C for 90 min. This reconstituted sample was then derivatized mixed with 50 µL N- (tert-butyldimethylsilyl)-N-methyltrifluoroacetamide (MTBSTFA) + 1% tert-butyldimethylchlorosilane (TBDMCS) and was derivatized at 70 °C for 30 min. The derivatized sample was filtered to get rid of insoluble salt due to residual medium or extraction before GC-MS runs. The prepared sample was eventually injected into a GC-MS, using dimethylformamide (DMF) as solvent (Sapcariu et al., 2014).

2.4. Quantification of mass isotopomer abundances and metabolite pool sizes by GC-MS analysis

All GC-MS analyses were performed on a Varian 300MS quadrupole GC-MS unit (Bruker Corporation, Fremont, CA) which is equipped with an autoinjector and a VF5-ms column of dimensions 0.25 mm × 30 m × 0.25 μm. During this study, 1 μL of derivatized soluble metabolites was automatically injected at a split ratio of 1:15 with helium as the carrier gas at a constant flow rate of 1.0 mL min^{-1}, with three technical replicates of each sample. For soluble metabolite analysis, the oven temperature procedure was set up holding an initial value at 150°C for 2 min, then with an increasing rate at 2°C min^{-1} to 175°C where it held the temperature for 2 min, and finally with an increasing rate at 3°C min^{-1} to 240°C for the rest of 38 min run time. The MS ran in electron ionization mode with a collection delay for 3 min. Mass spectra were recorded in the full scan mode or selected ion monitoring (SIM) mode. All mass spectral data were analyzed and quantified with the manufacturer's Varian MS Workstation software (Bruker, Billerica, MA).

2.5. Evaluation of data

Mass spectral data (CSV files exported from Varian software) were analyzed in MATLAB (The Mathworks, Natick, MA) using a MATLAB program developed by our group (Sriram et al., 2008), and we have verified its accuracy by previous utilization (specific data is not included). The program is designed to filter the natural abundances of elements which are not metabolic carbons. The mass isotopomer

distribution (MID) was obtained from the MATLAB program using singular value decomposition (SVD), abundances and enrichments were only obtained of the atoms or fragments that were calculable from the data. Also it is assumed that metabolic steady state was maintained during the instationary ILEs; therefore, flux values and metabolite pool sizes were constant in our model.

Chapter 3: Results

3.1. Preparation and optimization of modified L1 medium

3.1.1. Unlabeled modified medium

Before conducting the experiment, we had several different attempts towards the preparation of modified L1 medium. To minimize the change in growing environment, we kept the other components unaltered from L1 recipe provided by NCMA and planned to represent the trace metal (TM) component by combining all the chemicals listed in TM recipe. Due to vague description and demonstration about the concentration and amount of each metal ion provided by the L1 recipe (NCMA), it remained elusive for quite a spell before we could translate the recipe into practical procedure and operation. A number of trials were taken before stable TM stock solution was obtained.

There were circumstances when the stability of modified L1 medium reduced compared to pre-made original L1 medium, with higher possibility and shorter time for precipitating. However, the reason may be not about modification to TM component, since similar situation was observed later in our group with original L1 medium; therefore, we assume this was because of some issues with autoclave contaminating the seawater and container used throughout that trial.

Table 3 Typical trials in preparation of TM stock solution.
During the experiments, solid chemicals were purchased and used in the trials originally; later, solution of $ZnSO_4$ and $MnCl_2$ were directly purchased and put into use, in order to avoid precipitation at stock solution making stage. Several trials were made in order to maintain the other conditions the same as the TM stock solution provided by NCMA, such as color, pH, transparency. The most satisfactory method eventually turned out to be prepare the stock solution of each component and then combine them with calculated amount and add up to desired volume.

Trials taken in medium modification	**Result**
Mix solid chemicals before dissolved with deionized (DI) water	Fail
Mix other salts before adding Na_2EDTA into DI water	Fail
Dissolve each salt after Na_2EDTA in sequence	Fail
Prepare saturated stock solution from solid chemicals and mix in sequence	Fail
Replace some stock solution with purchased ones and combine saturated stock solutions and dilute enriched solution	Fail
Dilute stock solutions corresponding final concentration and make up with DI water	Success

3.1.2. ^{13}C labeled modified medium

Table 4 Investigation on proper bicarbonate concentration for ILEs.
Investigation was conducted using unlabeled ^{12}C bicarbonate. Besides the attempts in the table, a subculture with addition of bicarbonate were also conducted. Media with bicarbonate concentration more than 35g L^{-1} could hardly grow cells and no slight precipitation was observed in cultures in media with lower concentration. Even the medium could remain clear and stable with extra addition of Na_2EDTA, it was not adopted since Na_2EDTA is one of the component in L1 recipe and modifications to its concentration may have unknown effect on the incubation.

$NaHCO_3$ concentration	**Condition of dissolving**
40 g L^{-1}	Cannot dissolve after sufficient vortex
35 g L^{-1}	Fully dissolved with precipitate appear after 2 min's standing
30 g L^{-1}	Fully dissolved with precipitate appear after 10 min's standing
25 g L^{-1}	Fully dissolved with slight precipitation after 2 hours
20 g L^{-1}	Fully dissolved with slight precipitation after 6 hours
35 g L^{-1} with extra Na_2EDTA	Fully dissolved without precipitation after 24 hours

Note. Ambient temperature was between 25 to 30 ℃.

For ILEs conducted later in the research, a study of $NaHCO_3$ solubility in modified medium was conducted. Our group had experience running ILEs with 35 g L^{-1} $NaH^{13}CO_3$; therefore we set a concentration gradient around 35 g L^{-1}. It turned out

that the tolerance of modified medium for bicarbonate decreased in contrast to original formula, with precipitation appeared after 2 min's standing, and also we incubated subcultures in modified medium containing 35 g L^{-1} bicarbonate which turned out no growth and severe white deposition covering flask wall. After investigation given in Table. 4 and observation for 24 hours, 25 g L^{-1} was set to be the bicarbonate concentration in ILEs.

Despite the investigation discussed above, cells from five conditions were subcultured from incubation in unlabeled modified L1 medium (3.2.1) into corresponding modified L1 medium with same bicarbonate addition at concentration of 35 g L^{-1} and 30 g L^{-1} respectively. The suspensions were kept for a week and a large amount of white precipitation was observed adhering to the all flask walls. Cell counting results showed that hardly any cells grew in all flasks, indicating medium with these concentration levels were not fertile for *P. tricornutum* cells.

3.2. Cell growth experiments in modified L1 medium

3.2.1. Cell growth curve

Regular *P. tricornutum* cell culturing was conducted in the first stage. To investigate the Zn^{2+} effect on the photosynthesis efficiency, cell growth and cell reproduction, cell counting was conducted throughout the ordinary incubation, and the cell concentrations were calculated by General Method provided by INCYTO:

$\text{cells/ml} = \text{Average count/square} \times \text{dilution factor} \times \text{volume factor}(10^4)$ and given in the Table. 5.

Table 5 Average cell concentration and standard deviation.
Cell concentrations are average of calculation of three biological replicates from a same condition. Standard deviation are biological SDs calculated from two biological replicates from a same condition. Cell counting was conducted each day at a relatively fixed time so that the time comes in days rather than hours for simplicity. In order to obtain a clear view and comparison, the cell concentrations come in cells/μl instead of cells/ml. And also the cell concentrations referred to in the following all come in cells/μl. Significance test was performed using p value for conditions 2~5, between data from each condition and data from Condition 1. Results are shown in table using asterisk system.

Time (day)	Cell Concentration (cell/μl)									
	1	sd	2	sd	3	sd	4	sd	5	sd
3	215	67	353	51	260	50	190	22	433	46
6	4675	425	5200	250	5300	1500	5825	325	4775	1225
7	9650	150	9350	50	8400	1850	11800	1000	11550	2150
8	10800	700	9700	900	11950	450	12700	0	12150	550
9	11600	1000	13550	50	13900	2800	14150	150	14550	650
10	13200	200	*16200	400	16250	1950	*17250	450	*19050	650
13	15250	750	17000	0	17500	1000	18500	1000	*20000	500
14	18300	100	18600	0	19900	700	**19900	100	**21200	200
16	18100	1100	17000	400	19300	700	16900	1700	18300	300

Note. ** denotes p value <0.05 with respect to Condition 1*
***denotes p value <0.01 with respect to Condition 1*

Obtained data were plotted into Fig. 5. As can be seen from the diagram, cultures of various condition tended to reach a level with similar cell concentration after sufficient time (after 16 days). The similar final concentration may be due to same level of other nutrients in the modified L1 medium, such as nitrogen, phosphorus, silica and vitamins, indicating Zn^{2+} would not affect the cell's inquisition of other factors and reproduction level. However, differences were observed within the exponential growth state and cultures with higher Zn^{2+} level qualitatively tended to have higher cell concentration and growth rate, which may be a pointer that insufficiency in Zn^{2+} inhibits photosynthesis efficiency further leads to a slower cell growth rate.

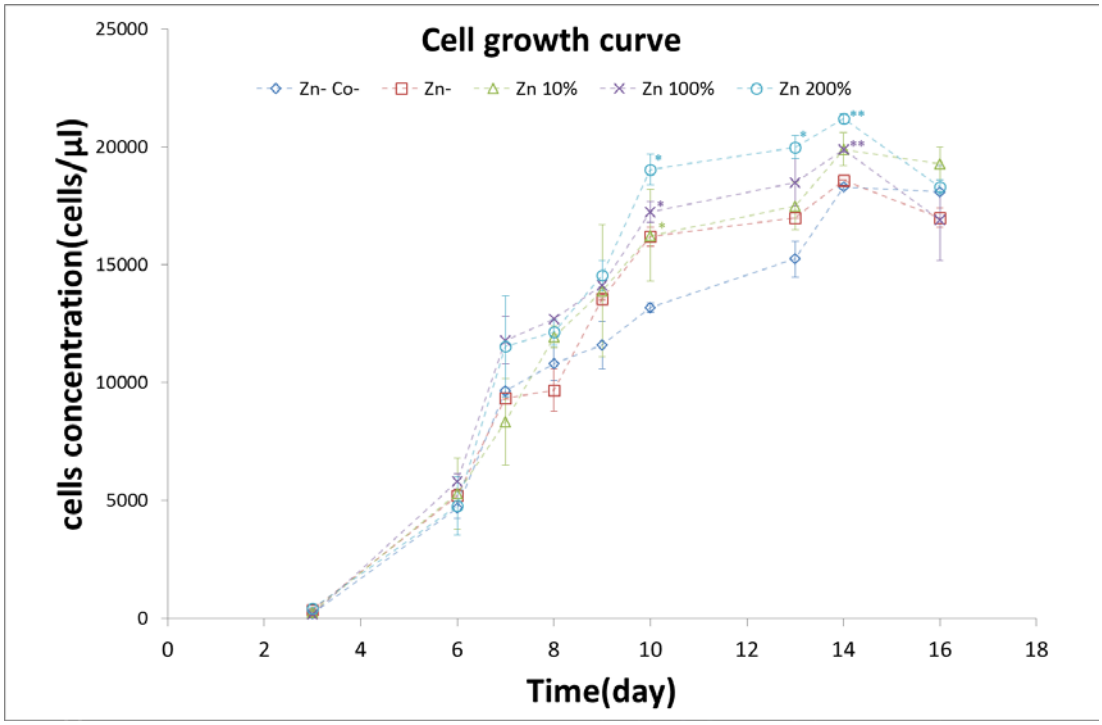

Figure 5 Cell growth curve with unlabeled carbon source.
Standard deviation are shown in vertical error bars. Condition 1: Zn- Zo-; Condition 2: Zn-; Condition 3: Zn 10%; Condition 4: Zn 100%; Condition 5: Zn 200%. The figure shows the changes in cell numbers of five different conditions, where it can be tell that disparity in cell number indeed occurred during the cell culture and decrease to vanish as time went by. Significance test was performed using *p* value for conditions 2~5 compared to data from Condition 1. Results are shown the figure using asterisk system, where * denotes $p < 0.05$ and ** denotes $p < 0.01$ with respect to Condition 1.

3.2.2. Linear fitting of exponential growth phase (Day 6~Day 13)

To better describe the cell concentration (x) within exponential growth phase quantitatively, we modeled x versus time (t) as follows:

$$x = x_0 e^{\mu t}$$

$$\mu = \frac{\mu_{\max}[s]}{K_m + [s]}$$

where x_0 is the initial cell concentration at $t = 0$;

K_m is a constant similar to the Monod constant for each condition;

s is a variable representing the nutrient level in the medium as a constraint;

μ is a function of [s];

μ_{max} is μ at exponential phase and could be considered constant.

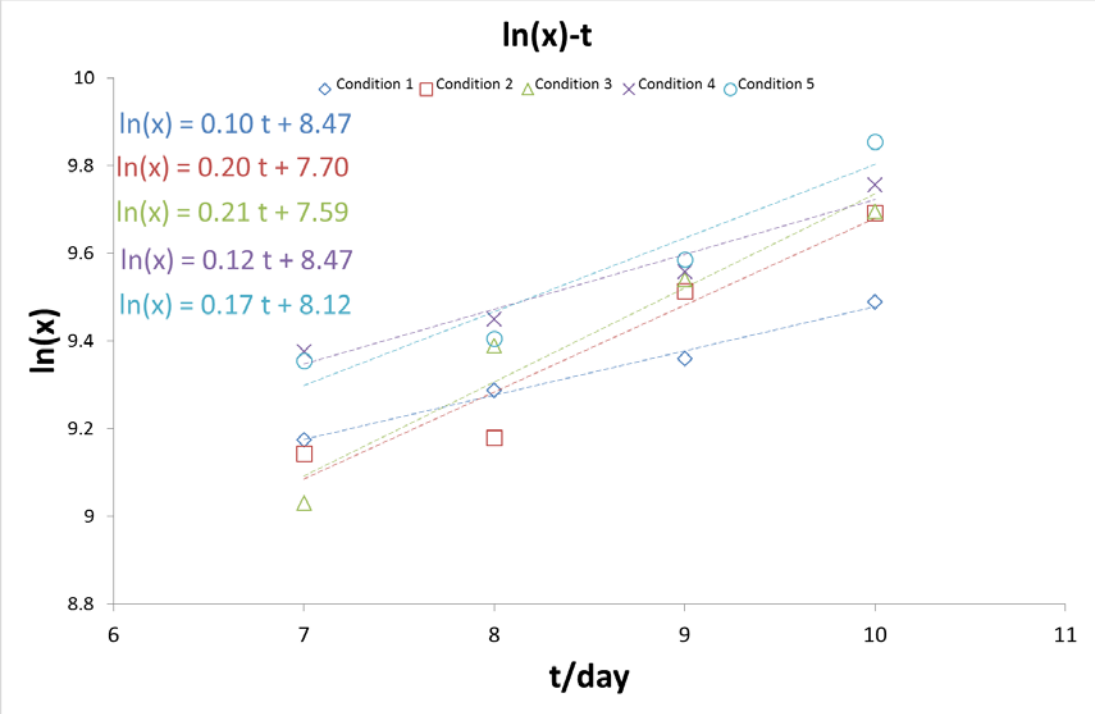

Figure 6 Linear fitted results of the exponential growth phase.
Markers in the figure stand for logarithm value of data at different time points. Lines stand for fitted equation $\ln(x) = a \times t + b$. Fitted function are given in the figure in order from Condition 1~5 and in corresponding color.

Cell numbers within exponential growth phase would fit in exponential growth function best with a rapid growth rate. Day 7-10 were chosen to conduct the linear fitting and results were shown in Table 6.

Fig. 5 and Fig. 6 can show that differences exist on both cell number and growth rate between the five conditions, although without a clear pattern; Fig. 5 also indicates

that conditions with slower growth rate can catch up with the ones with faster rate eventually. This proved our hypothesis where Zn^{2+} availability would have effect on CCMs and photosynthesis efficiency. It can be observed that the Zn^{2+} concentration mostly influence the growth rate, which is reasonable since major duty of CA is catalysis and cannot alone change the equilibrium of the reversible reaction between CO_2 and HCO_3^- without the help of putative carbon pumps or Zn-C assimilation as reported in other researches, changes in CA activity would have main effect on the kinetics instead of the final state of the reaction. Difference between Condition 1 and 2 also qualitatively indicates that Co^{2+} could replace Zn^{2+} when Zn^{2+} is insufficient.

Table 6 Results of fitted function $\ln(x) = a \times t + b$.
Linear fitting was performed using MATLAB function 'polyfit'. Variable *a* serves as slope while b serves intercept of the linear fitting, coefficient of determination (R^2) was calculated through equation $R^2 = 1 - SS_{residual} / SS_{total}$, in which $SS_{residual} = \sum (\text{estimated data - experimental data})^2$, and $SS_{total} = \sum (\text{experimental data - average value})^2$.
The degree of R^2's closeness to 1 reflects the closeness of fitted data to the experimental data. The fourth column is R^2 obtained from experimental data $\ln(x_i)$ and estimated data $\ln(x_{est}) = a \times t + b$; the fifth column is R^2 obtained from experimental data x_i and estimated data $x_{est} = \exp(a \times t + b)$. Both column show same degree of closeness between fitted data and experimental data of a same condition.

Condition	**Slope** ($a = \mu_{max}$)	**Intercept** ($b = \ln(x_0)$)	**R^2 from logarithm data point**	**R^2 from cell number**
Condition 1	0.10	8.47	0.99	0.99
Condition 2	0.20	7.70	0.93	0.96
Condition 3	0.21	7.59	0.95	0.96
Condition 4	0.12	8.47	0.95	0.97
Condition 5	0.17	8.12	0.92	0.95

However, no clear correlation between Zn^{2+} concentration and growth rate was observed. The reason may due to the difference in CA activities influenced cell growth and accelerated the approaching of exponential growth phase. Therefore

conditions with higher Zn concentration might have a faster rate approaching exponential growth phase earlier than Day 7-10.

Diversity can be seen between Condition 1 and Condition 2 while Condition 2 performed a higher growth rate than Condition 1, which may be possible that Co^{2+} acted as the substitution of Zn^{2+} in Condition 2.

Fig. 7 shows that the correlations between experimental data and estimated data of five different conditions are good using exponential growth function. Even though we still cannot exclude the probability that conditions containing higher Zn^{2+} concentration may have entered a state between exponential and stationary phases with decreasing growth rates.

Fig. 7

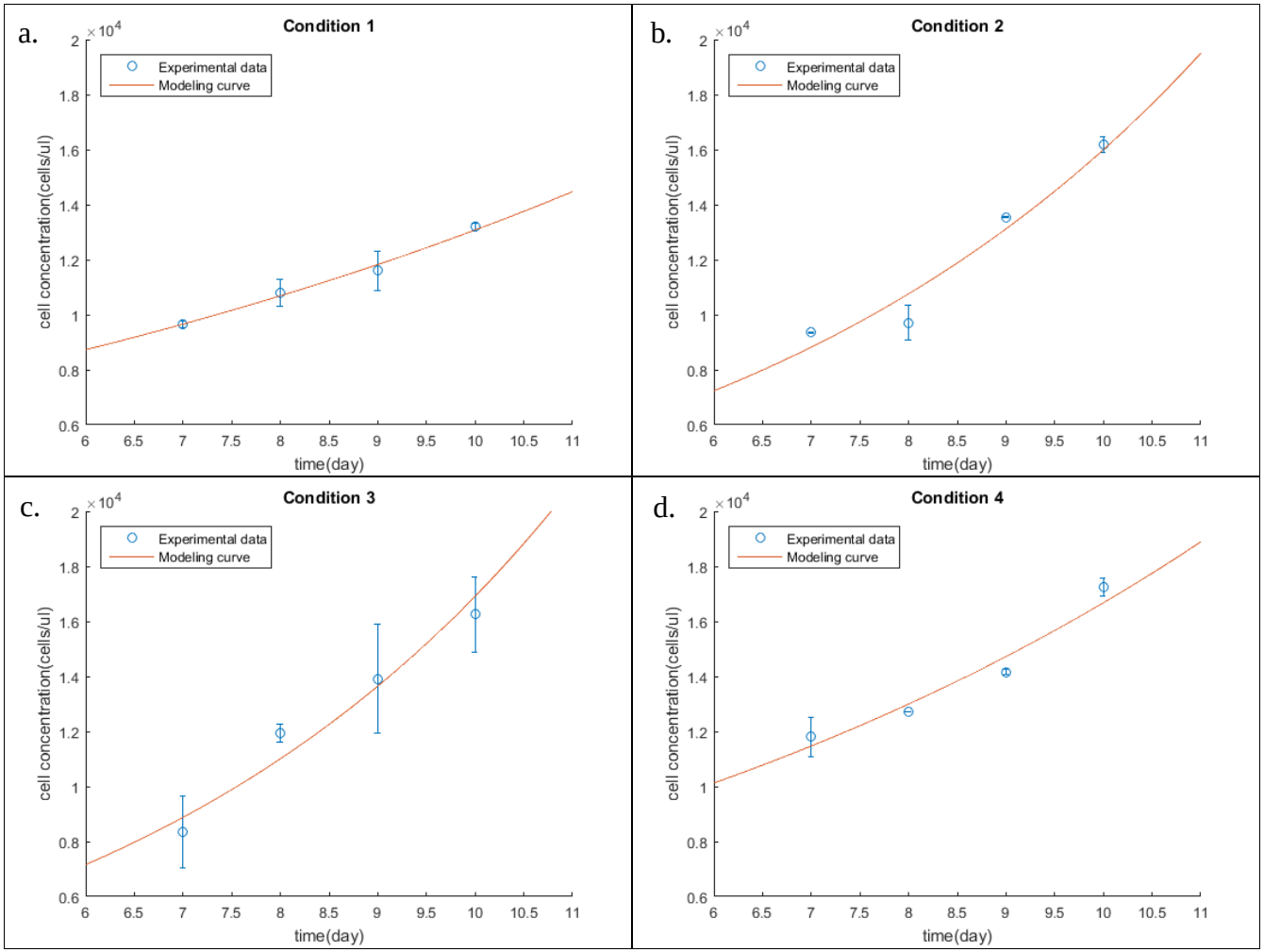
a.
Condition 1
b.
Condition 2
c.
Condition 3
d.
Condition 4
Experimental data
Modeling curve
cell concentration(cells/ul)
time(day)
×10^4

Figure continued

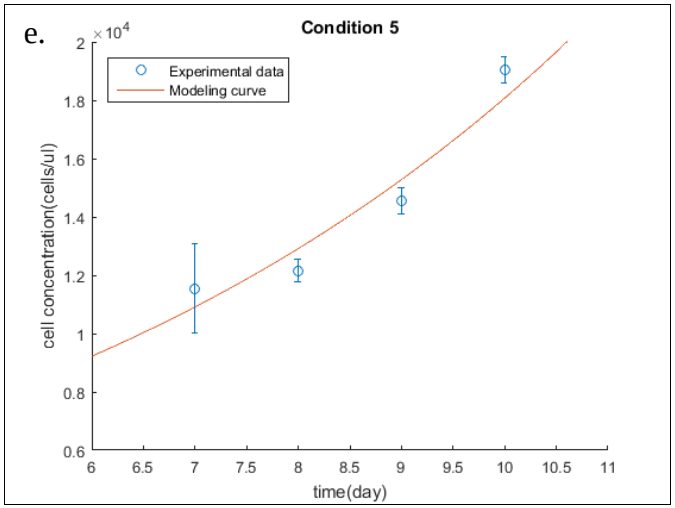

Figure 7 Experimental data and estimated data from linear fitting modeling.
(a) data from Condition 1; (b) data from Condition 2; (c) data from Condition 3; (d) data from Condition 4; (e) data from Condition 5. Colored markers represent experimental data and black markers represent estimated data from fitted function. Error bars show standard deviation from biological replicates.

3.2.3. Modeling over full time span

Next we fitted the modeling to the whole range of time rather than limited to exponential growth phase, the following ordinary differential equations (ODEs) were written:

$$\begin{cases} \dfrac{dx}{dt} = \mu x \\ \dfrac{d[s]}{dt} = -\dfrac{1}{yield} \times \dfrac{dx}{dt} \end{cases} \qquad (1)$$

where *yield* is value that can be estimated and is constant within each condition.

yield is related to the final cell concentration and the original nutrient contained in the medium, which draws connection between [*s*] and *x*. *yield* can be estimated using the following equation:

$$yield \approx \frac{x_{fin} - x_0}{s_0 - 0} \qquad (2)$$

Combine (1) and (2), and the ODE set was solved using in MATLAB.

Define $X = \begin{pmatrix} x \\ s \end{pmatrix}$ $\qquad \frac{dX}{dt} = \begin{pmatrix} \frac{dx}{dt} \\ \frac{ds}{dt} \end{pmatrix}$ $\qquad parameter = \begin{pmatrix} \mu_{\max} \\ K_m \\ x_{fin} \\ s_0 \\ x_0 \end{pmatrix}$

Function $\frac{dX}{dt}(X, t)$ is solved using function "ode45" with different input of array *parameter*. Chi-squared test was conducted after each run and iteration was performed to obtain minimum $\Delta\chi^2$ between two consecutive runs.

Five conditions have a same s_0 and x_0 denoting same nutrient level and cell concentration at Day 0. Estimated x_0 is close to the cell concentration from Day 0, which is calculated from cell concentration of original culture. In accordance of linear fitting result, modeling result shows a trend of ascending μ_{max} despite the variety to linear fitting result in quantitative values. Despite its deviation in linear fitting modeling, results of Condition 4 is following the putative rule among five conditions.

Table 7 Fitting result of cell growth data.
μ_{max}: maximal growth rate; K_m: half rate constant; x_{fin}: cell concentration at steady state; s_0: nutrient level at Day 0; x_0: cell concentration at Day 0; *SSR*: sum of squared errors calculated from $SSR = \sum(\text{estimated data} - \text{experimental data})^2 / SD^2$, where *SD* is standard deviation.
ODE sets was solved using "ode45" function. Chi-squared test was conducted and parameters were obtained through iteration.

Condition	μ_{max}	K_m	x_{fin}	s_0	x_0	*SSR*
Condition 1	0.387	0.0024	18536			4648
Condition 2	0.391	0.0041	18627			64465
Condition 3	0.427	0.0052	19982	0.865	114	424
Condition 4	0.445	0.0046	21016			77528
Condition 5	0.497	0.0068	20397			309

K_m is the value of [*s*] at the point when the cells had a growth rate that equals $1/2\mu_{max}$. A higher K_m means the system reaches the $1/2\mu_{max}$ while other nutrients are at a higher level, indicating a faster approach of exponential growth phase and steady state, and vice versa. K_m of five conditions also showed increasing pattern from Condition 1 to 5, which is solid through our qualitative observation from cell growth curve.

x_{fin} is the cell concentration at steady state (t_{ss}) and t_{ss} was set to 20 days during the calculation. Alike x_{fin}s were obtained from the modeling, which proves our hypothesis of Zn^{2+} does not affect the final cell concentrations.

The modeling result is consistent with our observations and hypotheses from both cell growth curve and linear fitting result, illustrating that condition with higher Zn^{2+} availability would have higher growth rate and the time approaching steady state would be shorten, also the Zn^{2+} does not have influence on the cell concentrations at steady state.

Figure 8

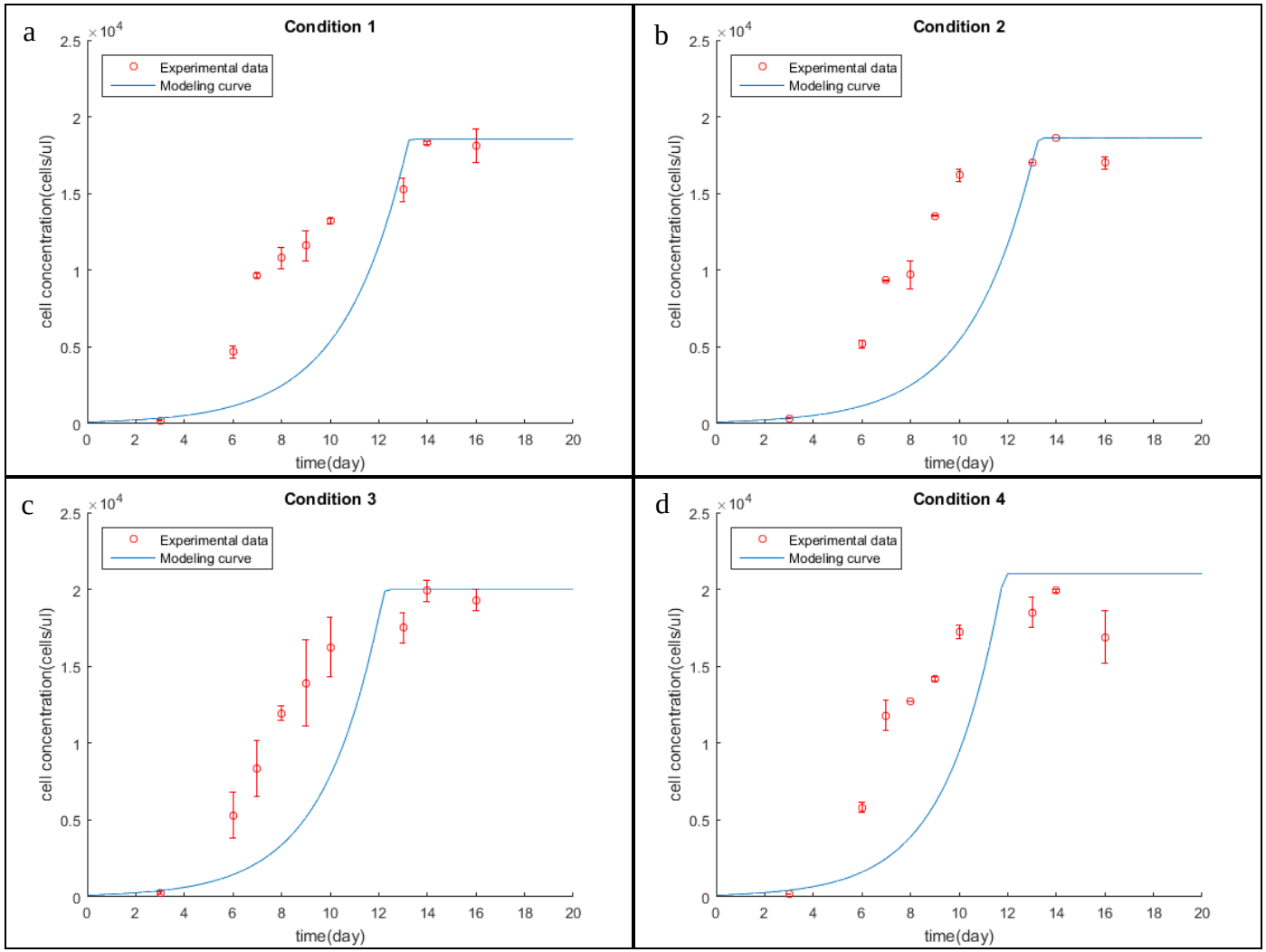
a
Condition 1
b
Condition 2
c
Condition 3
d
Condition 4
Experimental data
Modeling curve
cell concentration(cells/ul)
time(day)
×10^4

Figure continued

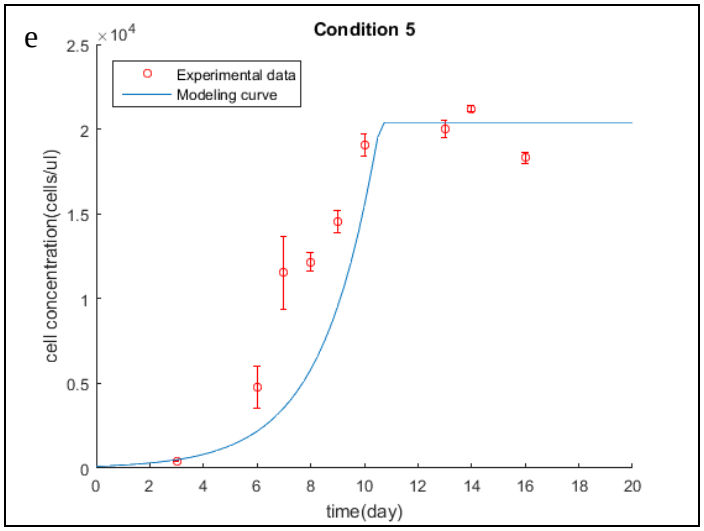

Figure 8 Experimental data and estimated data from non-linear fitting modeling.
(a) data from Condition 1; (b) data from Condition 2; (c) data from Condition 3; (d) data from Condition 4; (e) data from Condition 5. Round markers represent experimental data and smooth line represent modeling curve from fitted function. Error bars show standard deviation from biological replicates.

3.3. Instationary ILEs results

Conclusion was drawn from previous investigation that maximal differences of cell growths and concentrations appear within 9~15 days after subculture, which is also within the exponential growth phase. To better examine the ability of carbon assimilation by *P. tricornutum*, short-time and long-time ILEs were conducted at time point of 12 days growth by adding supplemental $H^{13}CO_3^-$ in modified L1 medium. Short time experiments were conducted in micro-centrifuge tubes with time range from 1 min to 30 min, when cells were transferred into medium with addition of 25 g L^{-1} $NaH^{13}CO_3$. Long time experiments were conducted in Erlenmeyer flasks for 4 hours and 8 hours, with same total amount of $NaH^{13}CO_3$ supplemented into medium. Condition 1, 3 and 5 were chosen to conduct the ILEs also in order to maximize the differences between the cultures. Original 1 ml of the L1 medium was secondary diluted into 1/2500 and the Zn^{2+} and Co^{2+} component from regular recipe was minimized, also natural abundance of Zn^{2+} and Co^{2+} in sea water can be ignored as mentioned above.

After cell harvesting, soluble intracellular metabolites were extracted from the cell suspension by decomposing cell wall and structure with methanol. Isolated soluble metabolites were quantified using GC-MS tests and mass isotopomer distribution (MID) and ^{13}C enrichment were obtained. The results serve as strong pointer for our hypothesis and conclusion from above.

3.3.1. MID of Mal [1234] (m+1)

A mass spectrum of a sample is a pattern representing the distribution of mass-charge ratio (*m*/*z*). Background noise and natural abundance of atoms other than metabolic carbons that we are interested in can be extracted along with valuable peaks during data export, which calls for a filtration of raw data. A program designed by our group (Sriram et al., 2008) was applied to the convert the raw data into MID files as well as ^{13}C enrichments. MID data shows directions of isotopes heading and can be used in metabolic flux analysis.

Table 8 Proteinogenic amino acids derived from fragments.

Fragment	**Proteinogenic amino acid**	**Fragment**	**Proteinogenic amino acid**
OAA	Asp	PEP	Phe and Tyr
α-ketoglutarate (αKG)	Glu	Pyr	Ala and Val
3PG	Ser and Gly		

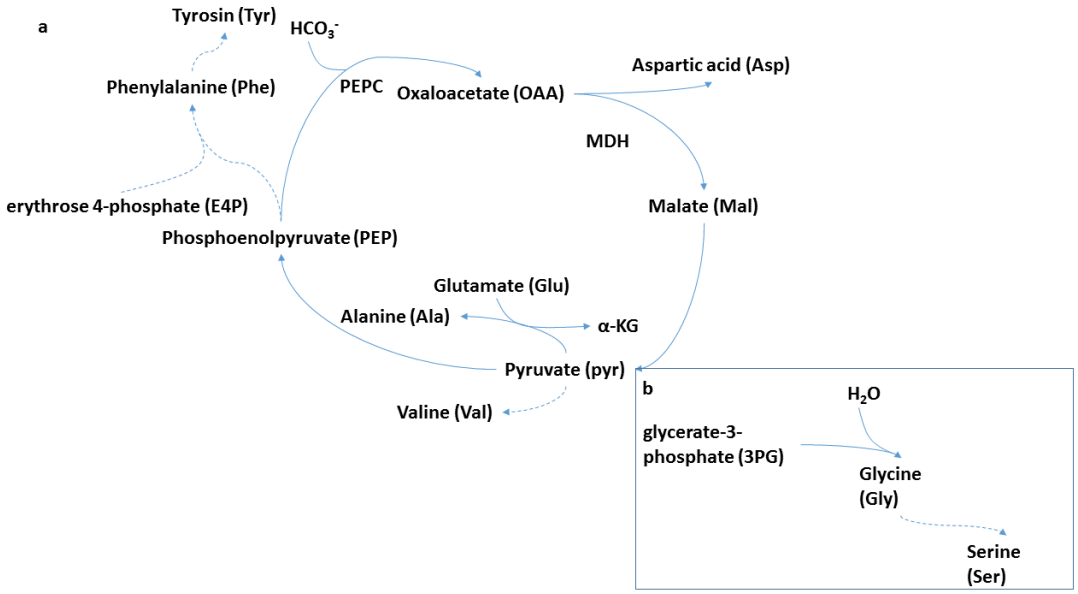

Figure 9 Correlations of proteinogenic amino acid and important metabolites. (a) Amino acid derived from C_4 pathway; (b) Gly and Ser derived from 3PG. Solid line: through direct reaction; dashed line: through multiple reaction or pathways.

The abundances of isotopomers of fragments or atoms that are important from central carbon metabolites could be estimated retro-biosynthetically from proteinogenic amino acids derived from them. The abundances information can be utilized in the analysis of mechanism of biochemical pathway, illustrating the way CO_2 is captured into C_4 compound and C_4 pathway. Table 8 and Fig. 9 both showed the relation of amino acids and important metabolites inside the cell; therefore isotopomer abundances and ^{13}C enrichments of these fragments could reflect the carbon flux from instationary ILEs. For example, OAA and Mal are two important C_4 compounds CO_2 is incorporated into, hence data of Asp fragments (downstream metabolite derived from OAA) and Mal fragments were especially analyzed; same situation also applies for Ala, Glu, Gly, Ser, Phe, Tyr, Val, etc. during the analysis.

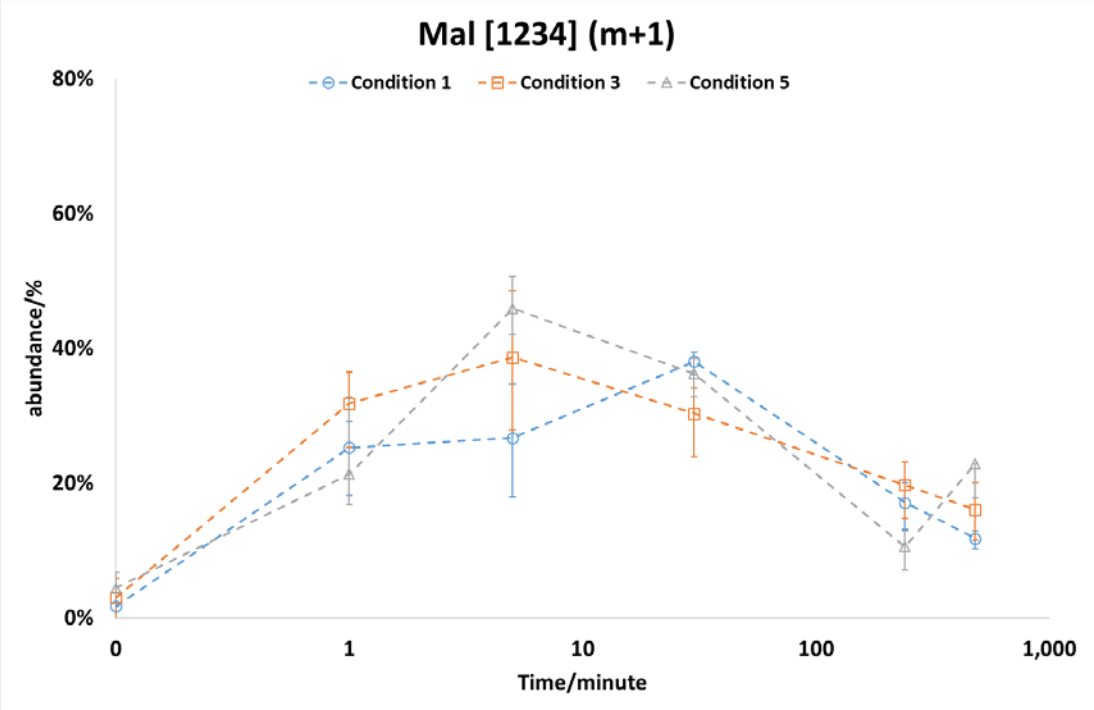

Figure 10 Abundance of Mal [1234] (m+1) fragment.
Blue markers: Condition 1, orange markers: Condition 3, gray markers: Condition 5. Positive vertical error bar shows standard error caused by technical runs, negative vertical error bar shows standard error resulted by biological replicates.

Abundances in Mal [1234] (m+1) does not show much disparity among the three conditions according to Fig. 10. On the premise that *P. tricornutum* can complete C_4 CCMs, alike abundances may indicate the similar level of C_4 CCMs.

Even though 1 min and 5 min abundances tend to have increased diversity related to time, the data were obtained from such short-time experiments that the experiment can be interfered by many factors and the environments were intensively unsteady, therefore the short-time data could have relatively high standard deviations (SD) and are less persuasive than 4 hour and 8 hour ones.

3.3.2. MID of Asp fragments

Many fragments of Aspartic acid can be detected in mass spectrometry; however, due to low biomass and cell concentration, we would focus on Asp [12] (m+1) and Asp [234] (m+1) fragments. Three conditions turned out to share an alike curve shown in Fig. 11 (a) and (b). MID of Asp [12] is shown in Fig. 12, from which one can observe that the conclusions drawn from analysis of three fragments were consistent, that is, three conditions do not have significant diversities in MID of Asp fragment, indicating the differences in OAA abundance and concentration among three condition were insignificant.

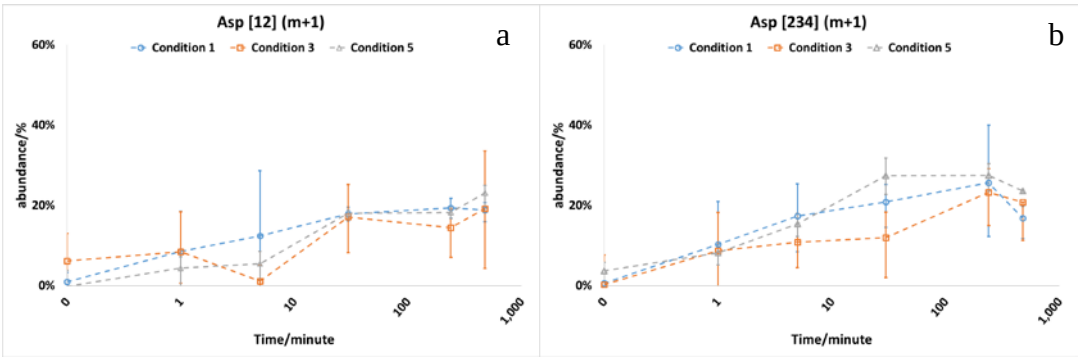

Figure 11 Abundance of Asp fragments.
(a) abundances of fragment Asp [12] (m+1) versus time; (b) abundances of fragment Asp [234] (m+1) versus time. Blue markers: Condition 1, orange markers: Condition 3, gray markers: Condition 5. Positive vertical error bar shows standard error caused by technical runs, negative vertical error bar shows standard error resulted by biological replicates.

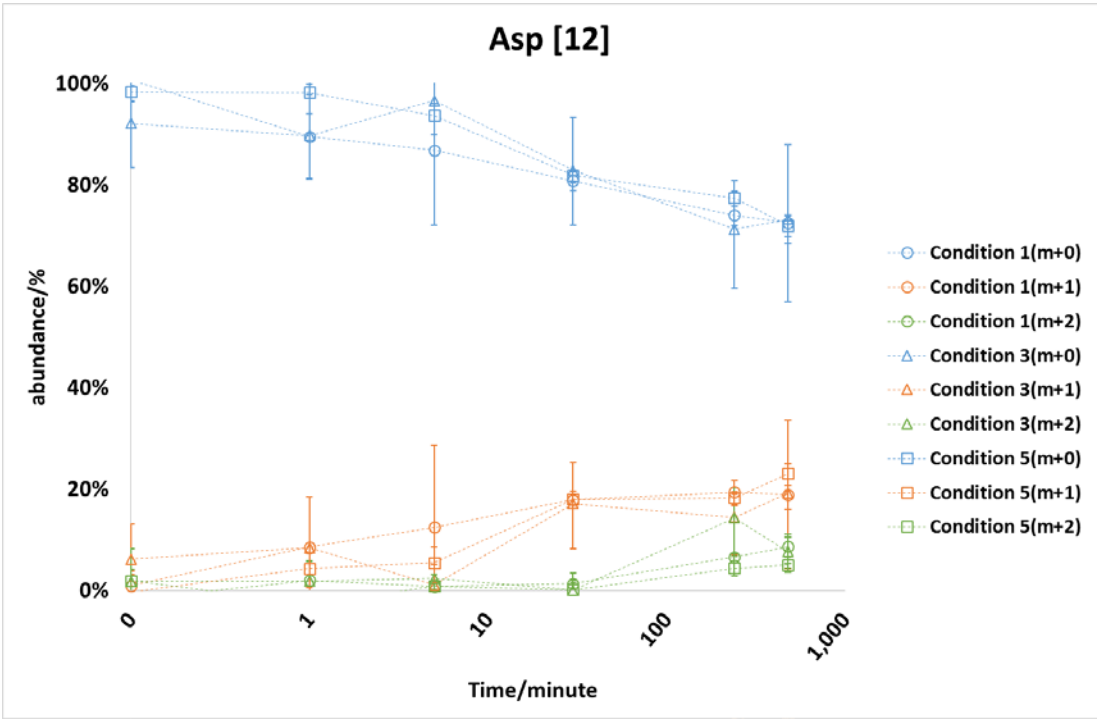

Figure 12 MIDs of Asp [12] fragment.
Blue markers: Asp [12] fragment with mass (m+0), orange markers: Asp [12] fragment with mass (m+1), green markers: Asp [12] fragment with mass (m+2). Round markers: Condition1, triangle markers: Condition 3,
square markers: Condition 5. Positive vertical error bar shows standard error caused by technical runs, negative vertical error bar shows standard error resulted by biological replicates.

Throughout more analysis of the abundances and ^{13}C enrichments (not included in this paper), no markedly contrast was observed among the three conditions for the metabolite carbons that were calculable. Many of the calculable carbons and fragments are important intermediate products (such as Mal) or downstream products (such as Asp) that are valuable in analysis of C_4 CCMs; however, the abundances of the fragments tended to have similar values and changing trends versus time, indicating the biochemical CCMs level in three different conditions did not have remarkable variety. It can be considered negative result of the ILEs, and this conclusion conflicts with our assumption that low level of biophysical CCMs inhibited by low CA activity might result in prompt in C_4 CCMs; hence, it may be because the Zn^{2+} concentration does not have much influence on C_4 CCMs and not correspondences between biophysical and biochemical CCMs is observed in the investigation.

A possible reason for this observation may be caused by addition of $H^{13}CO_3^-$, since the concentration of $H^{13}CO_3^-$ is significantly higher than that of ambient marine and L1 environment, which means equilibrium between C_4 compound (OAA) and $H^{13}CO_3^-$ catalyzed by PEPC would largely favor OAA direction. The effect of high $H^{13}CO_3^-$ on the equilibrium overcame probable effect of Zn^{2+} such as compensation for biophysical CCMs, therefore Zn^{2+} turned out to have no obvious effect throughout the research according to GC-MS results.

Another possible reason for the phenomena is that when bicarbonate was added into the medium, it did not only introduced in HCO_3^-, but would also enhanced the CO_2 concentration in the medium and partial pressure of the environment inside the flasks

and tubes due to decomposition. Higher CO_2 concentration would disfavor the conversion of CO_2 towards HCO_3^- by CA, resulting in inhibition and lower ability of CA. Therefore the insignificant differences in the ILEs may be due to CAs' low activities in all three conditions.

MID data of Alanine and Aspartic acid of Condition 1 are given in Appendix A for supplementary demonstration, more data are not included in this paper.

Chapter 4: Discusion

The differences caused by Zn^{2+} level between cultures of five conditions of various media appeared at early stage of incubation, expanded along with growth and fade away after exponential growth phase. The similar final cell concentration indicates that the CA activity mainly affects kinetics of the cell growth instead of steady states. Even though it showed no obvious disparity in long term growth, Zn^{2+} indeed influences the cell growth rate and can decrease the time needed to reach final cell concentration level, indicating its influence on the cell metabolism. There is evidence showing that *P. tricornutum* cells treated with CA inhibitor tended to have a lower maximal photosynthetic rate (Satoh, Hiraoka, Colman, & Matsuda, 2001), which is qualitatively consistent with our result. The experiments can be also indirectly correlated to the previous study showing that low CO_2 concentration calls for a higher Zn intake (Sunda & Huntsman, 2005), also with the conclusion that CA activity depends on Zn^{2+} concentration after induced by low CO_2 concentration (Lane & Morel, 2000). Utilization of this observation could shorten the growth cycle and the time for cells to reach a maximal concentration in regular environment without demand on higher nutrition levels.

While the concentration changes had major effect on the kinetics of cell growth, we observed that the effect mainly acts on biophysical CCMs through analysis of data from isotope labeling experiments. ILEs showed that C_4 CCMs of the three conditions operated similarly and the differences among them were not significant. The experiments showed no compensation prompt in C_4 CCMs, and this is conflict

with what we hypothesized before the research. It is possible that Zn^{2+} concentration indeed have no effect on C_4 pathway and the putative compensation does not exist, indicating that the cells do not regulate between two kinds of CCMs even both mechanism are performed in *P. tricornutum* cells (Badger & Price, 1994; Harada & Matsuda, 2005; Kroth et al., 2008). If this assumption of explanation is proven, that is, Zn^{2+} concentration would not affect the C_4 pathways, indicating that Zn^{2+} level can be used to accelerate cell growth without disturbing patterns of intracellular metabolite distribution. Another possible reason is that high HCO_3^- concentration caused by addition of bicarbonate forced the equilibrium between HCO_3^- and C_4 compound significantly tilts to OAA/Mal direction, especially in short time ILEs. The strong effect of high HCO_3^- concentration may have overcome any probable effect brought in by Zn^{2+}. It is also possible that extra bicarbonate addition increased the CO_2 concentration through equilibrium of carbon dissociation in the medium, resulting in an unfavorable condition of CA converting HCO_3^- into CO_2 for accumulation, equivalently the CA ability was inhibited (Sunda & Huntsman, 2005). This assumption can be further investigated using different kinds of inorganic carbon isotopes.

Besides, in order to conduct the ILEs at maximal contrast between the cultures, the experiments were conducted on cells only incubated for 12 days after subculture, when both cell concentration and biomass were not quite amplified. It cannot be denied that insufficient biomass increased the difficulty of data analysis, for some signals were so low and so close to noise that they could not be calculable, they might had negative impact on the investigation. Even though it is unlikely to affect the

conclusion about correlation between biophysical and C_4 CCMs, low biomass and cell numbers may have impacted the investigations and analyses of C_4 CCMs.

From above discussion, our future study would come in the following aspects. (1) With the obtained data, reduplicative GC-MS test will be performed with lower split ratio, so as to obtain result with less interference from the noise and might make more metabolites calculable and reduce technical and biological standard deviation. (2) For less negative influence of noise and relatively lower standard deviation, ILEs can be conducted onto the cells with sufficient biomass and cell number. The MID pattern would show differences between conditions as well since the Zn^{2+} has impact on the kinetics of CCMs and photosynthesis metabolism. GC-MS tests of ILEs on cells sufficient biomass would have improved results, because the peaks would be higher than that of ones have insufficient biomass and would be significantly difference from noise and more calculable. (3) In order to avoid high $H^{13}CO_3^-$ concentration introduced by addition of bicarbonate, we would first culture *P. tricornutum* cells in labeled modified L1 medium for adequate time to steady state so that we can consider the metabolites involved in photosynthesis and downstream pathways are fully labeled. The cells will then be transferred into unlabeled medium to conduct ILEs with ^{12}C as labeling isotope. This study would reveal the effect of Zn^{2+} on C_4 CCMs under ambient CO_2 and $H^{13}CO_3^-$ concentration rather than high concentration in the study above. (4) Photorespiration favors O_2 over 30 °C (Parker & Armbrust, 2005), indicating temperature is playing an important role in photosynthesis. Experiments can be conducted under relatively low temperature to investigate the photosynthetic efficiency when O_2 is not strongly competitive for RuBisCO.

Appendix A

Appendix A. MIDs for Ala and Asp fragments of Condition 1

Time (min)				0						1					
AA	frag	MW-frag	n (m+n)	adjusted abundance	technical SD	biological SD	13C enrichment	technical SD	biological SD	adjusted abundance	technical SD	biological SD	13C enrichment	technical SD	biological SD
Ala	[23]	232	0	0.98	0.01	0.01	0.7	0.2	0.7	0.98	0.09	0.06	0.4	1.8	4.1
Ala	[23]	232	1	0.02	0.01	0.01				0.04	0.05	0.04			
Ala	[23]	232	2	0.00	0.01	0.01				0.00	0.04	0.03			
Ala	[123]	260	0	0.98	0.05	0.03	0.5	0.4	1.2	0.94	0.07	0.05	3.4	2.3	3.4
Ala	[123]	260	1	0.03	0.04	0.03				0.04	0.06	0.04			
Ala	[123]	260	2	0.00	0.02	0.01				0.00	0.03	0.03			
Ala	[123]	260	3	0.00	0.01	0.01				0.02	0.03	0.03			
Asp	[12]	302	0	1.01	0.11	0.07	0.1	2.8	5.4	0.89	0.25	0.14	6.3	5.6	8.4
Asp	[12]	302	1	0.01	0.07	0.06				0.09	0.30	0.16			
Asp	[12]	302	2	0.00	0.05	0.04				0.02	0.12	0.07			
Asp	[234]	316	0	0.96	0.18	0.09	4.2	3.6	5.8	0.76	0.21	0.19	17.5	11.2	14.7
Asp	[234]	316	1	0.01	0.10	0.07				0.10	0.32	0.21			
Asp	[234]	316	2	0.00	0.07	0.04				0.00	0.16	0.11			
Asp	[234]	316	3	0.04	0.08	0.05				0.14	0.25	0.17			
Asp	[234]	390	0	0.97	0.08	0.05	1.5	1.2	2.8	0.85	0.27	0.27	9.7	13.4	12.6
Asp	[234]	390	1	0.02	0.12	0.08				0.01	0.35	0.18			
Asp	[234]	390	2	0.02	0.08	0.07				0.15	0.34	0.27			
Asp	[234]	390	3	0.00	0.02	0.02				0.00	0.23	0.11			

Table continued

Time (min)				5						30					
AA	frag	MW-frag	n (m+n)	adjusted abundance	technical SD	biological SD	13C enrichment	technical SD	biological SD	adjusted abundance	technical SD	biological SD	13C enrichment	technical SD	biological SD
Ala	[23]	232	0	0.98	0.03	0.02	1.2	0.7	1.7	0.95	0.05	0.03	2.7	1.6	2.1
Ala	[23]	232	1	0.02	0.03	0.02				0.04	0.04	0.03			
Ala	[23]	232	2	0.00	0.02	0.01				0.01	0.01	0.01			
Ala	[123]	260	0	0.93	0.04	0.04	2.6	1.0	1.6	0.93	0.02	0.14	2.6	0.4	4.5
Ala	[123]	260	1	0.07	0.06	0.04				0.06	0.03	0.15			
Ala	[123]	260	2	0.00	0.04	0.03				0.00	0.02	0.03			
Ala	[123]	260	3	0.01	0.01	0.01				0.00	0.01	0.01			
Asp	[12]	302	0	0.87	0.42	0.26	6.9	7.8	11.5	0.81	0.05	0.03	10.3	1.3	2.2
Asp	[12]	302	1	0.12	0.49	0.29				0.18	0.05	0.03			
Asp	[12]	302	2	0.01	0.07	0.05				0.01	0.02	0.02			
Asp	[234]	316	0	0.65	0.35	0.25	21.7	12.6	16.0	0.77	0.12	0.09	8.2	1.6	2.6
Asp	[234]	316	1	0.17	0.24	0.15				0.21	0.13	0.11			
Asp	[234]	316	2	0.05	0.43	0.23				0.01	0.05	0.03			
Asp	[234]	316	3	0.13	0.10	0.06				0.00	0.02	0.01			
Asp	[234]	390	0	0.82	0.00	0.16	6.2	1.9	5.8	0.75	0.03	0.02	9.1	0.9	1.6
Asp	[234]	390	1	0.17	0.00	0.19				0.24	0.05	0.03			
Asp	[234]	390	2	0.00	0.00	0.09				0.01	0.04	0.03			
Asp	[234]	390	3	0.01	0.00	0.02				0.01	0.03	0.02			

Table continued

Time (min)				240						480					
AA	frag	MW-frag	n (m+n)	adjusted abundance	technical SD	biological SD	13C enrichment	technical SD	biological SD	adjusted abundance	technical SD	biological SD	13C enrichment	technical SD	biological SD
Ala	[23]	232	0	0.79	0.03	0.12	14.0	0.6	7.7	0.77	0.06	0.04	15.3	1.2	2.6
Ala	[23]	232	1	0.15	0.03	0.09				0.16	0.04	0.03			
Ala	[23]	232	2	0.07	0.01	0.03				0.07	0.02	0.01			
Ala	[123]	260	0	0.69	0.02	0.02	15.3	0.9	0.9	0.64	0.09	0.07	17.7	1.1	3.2
Ala	[123]	260	1	0.18	0.02	0.01				0.22	0.06	0.04			
Ala	[123]	260	2	0.10	0.01	0.01				0.11	0.04	0.03			
Ala	[123]	260	3	0.03	0.01	0.00				0.03	0.01	0.01			
Asp	[12]	302	0	0.74	0.05	0.04	16.3	1.7	1.9	0.72	0.05	0.05	18.1	1.9	3.3
Asp	[12]	302	1	0.19	0.07	0.04				0.19	0.06	0.05			
Asp	[12]	302	2	0.07	0.02	0.02				0.09	0.06	0.04			
Asp	[234]	316	0	0.62	0.32	0.21	17.6	7.1	7.8	0.74	0.09	0.06	12.1	1.5	2.5
Asp	[234]	316	1	0.26	0.43	0.23				0.17	0.09	0.09			
Asp	[234]	316	2	0.10	0.16	0.09				0.07	0.04	0.03			
Asp	[234]	316	3	0.02	0.04	0.03				0.02	0.02	0.01			
Asp	[234]	390	0	0.71	0.07	0.07	15.6	1.0	2.2	0.65	0.06	0.06	13.2	0.1	1.6
Asp	[234]	390	1	0.16	0.08	0.07				0.30	0.10	0.09			
Asp	[234]	390	2	0.08	0.04	0.04				0.04	0.05	0.04			
Asp	[234]	390	3	0.05	0.04	0.04				0.01	0.05	0.04			

Bibliography

Badger, M. R., Andrews, T. J., Whitney, S. M., Ludwig, M., Yellowlees, D. C., Leggat, W., & Price, G. D. (1998). The diversity and coevolution of Rubisco, plastids, pyrenoids, and chloroplast-based CO2-concentrating mechanisms in algae. *Canadian Journal of Botany*, *76*(6), 1052–1071.

Badger, M. R., & Price, G. D. (1994). The role of carbonic anhydrase in photosynthesis. *Annual Review of Plant Biology*, *45*(1), 369–392.

Borowitzka, M. A., & Volcani, B. E. (1978). The Polymorphic Diatom Phaeodactylum Tricornutum: Ultrastructure of Its Morphotypes. *Journal of Phycology*, *14*(1), 10–21.

Bowler, C., Allen, A. E., Badger, J. H., Grimwood, J., Jabbari, K., Kuo, A., … others. (2008). The Phaeodactylum genome reveals the evolutionary history of diatom genomes. *Nature*, *456*(7219), 239–244.

Diatom. (2015, November 20). In *Wikipedia, the free encyclopedia*. Retrieved from https://en.wikipedia.org/w/index.php?title=Diatom&oldid=691469091

Doan, T. T. Y., Sivaloganathan, B., & Obbard, J. P. (2011). Screening of marine microalgae for biodiesel feedstock. *Biomass and Bioenergy*, *35*(7), 2534–2544.

Dugdale, R. C., & Wilkerson, F. P. (1998). Silicate regulation of new production in the equatorial Pacific upwelling. *Nature*, *391*(6664), 270–273.

Ellis, R. J. (2010). Biochemistry: Tackling unintelligent design. *Nature*, *463*(7278), 164–165.

Falkowski, P. G., & Raven, J. A. (2013). *Aquatic photosynthesis*. Princeton University Press.

Goldman, J. C., McGillicuddy Jr, D., & others. (2003). Effect of large marine diatoms growing at low light on episodic new production. *Limnology and Oceanography*, *48*(3), 1176–1182.

Haimovich-Dayan, M., Garfinkel, N., Ewe, D., Marcus, Y., Gruber, A., Wagner, H., … Kaplan, A. (2013). The role of C4 metabolism in the marine diatom Phaeodactylum tricornutum. *New Phytologist*, *197*(1), 177–185.

Harada, H., & Matsuda, Y. (2005). Identification and characterization of a new carbonic anhydrase in the marine diatom Phaeodactylum tricornutum. *Canadian Journal of Botany*, *83*(7), 909–916.

Kitao, Y., Harada, H., & Matsuda, Y. (2008). Localization and targeting mechanisms of two chloroplastic β-carbonic anhydrases in the marine diatom Phaeodactylum tricornutum. *Physiologia Plantarum*, *133*(1), 68–77.

Kroth, P. G., Chiovitti, A., Gruber, A., Martin-Jezequel, V., Mock, T., Parker, M. S., … others. (2008). *A model for carbohydrate metabolism in the diatom Phaeodactylum tricornutum deduced from comparative whole genome analysis*. Bibliothek der Universität Konstanz. Retrieved from http://dx.plos.org/10.1371/journal.pone.0001426

Lane, T. W., & Morel, F. M. (2000). Regulation of carbonic anhydrase expression by zinc, cobalt, and carbon dioxide in the marine diatom Thalassiosira weissflogii. *Plant Physiology*, *123*(1), 345–352.

Lane, T. W., Saito, M. A., George, G. N., Pickering, I. J., Prince, R. C., & Morel, F. M. (2005). Biochemistry: a cadmium enzyme from a marine diatom. *Nature*, *435*(7038), 42–42.

Lewin, J. C., Lewin, R. A., & Philpott, D. E. (1958). Observations on Phaeodactylum tricornutum. *Journal of General Microbiology*, *18*(2), 418–426.

Marchetti, A., Maldonado, M. T., Lane, E. S., & Harrison, P. J. (2006). Iron requirements of the pennate diatom Pseudo-nitzschia: Comparison of oceanic (high-nitrate, low-chlorophyll waters) and coastal species. *Limnology and Oceanography*, *51*(5), 2092–2101.

Morel, F. M. M., Reinfelder, J. R., Roberts, S. B., Chamberlain, C. P., Lee, J. G., & Yee, D. (1994). Zinc and carbon co-limitation of marine phytoplankton. *Nature*, *369*(6483), 740–742.

Parker, M. S., & Armbrust, E. (2005). Synergistic effects of light, temperature, and nitrogen source on transcription of genes for carbon and nitrogen metabolism in the centric diatom Thalassiosira pseudonana (bacillariophyceae). *Journal of Phycology*, *41*(6), 1142–1153.

Parker, M. S., Armbrust, E., Piovia-Scott, J., & Keil, R. G. (2004). Induction of photorespiration by light in the centric diatom Thalassiosira weissflogii (bacillariophyceae). *Journal of Phycology*, *40*(3), 557–567.

Raven, J. A. (2010). Inorganic carbon acquisition by eukaryotic algae: four current questions. *Photosynthesis Research*, *106*(1-2), 123–134.

Rech, M., Morant-Manceau, A., & Tremblin, G. (2008). Carbon fixation and carbonic anhydrase activity in Haslea ostrearia (Bacillariophyceae) in relation to growth irradiance. *Photosynthetica*, *46*(1), 56–62.

Reinfelder, J. R. (2011). Carbon concentrating mechanisms in eukaryotic marine phytoplankton. *Marine Science*, *3*.

Reinfelder, J. R., Kraepiel, A. M., & Morel, F. M. (2000). Unicellular C4 photosynthesis in a marine diatom. *Nature*, *407*(6807), 996–999.

Reinfelder, J. R., Milligan, A. J., & Morel, F. M. (2004). The role of the C4 pathway in carbon accumulation and fixation in a marine diatom. *Plant Physiology*, *135*(4), 2106–2111.

Roberts, K., Granum, E., Leegood, R. C., & Raven, J. A. (2007a). C3 and C4 pathways of photosynthetic carbon assimilation in marine diatoms are under genetic, not environmental, control. *Plant Physiology*, *145*(1), 230–235.

Roberts, K., Granum, E., Leegood, R. C., & Raven, J. A. (2007b). Carbon acquisition by diatoms. *Photosynthesis Research*, *93*(1-3), 79–88.

Sapcariu, S. C., Kanashova, T., Weindl, D., Ghelfi, J., Dittmar, G., & Hiller, K. (2014). Simultaneous extraction of proteins and metabolites from cells in culture. *MethodsX*, *1*, 74–80.

Satoh, D., Hiraoka, Y., Colman, B., & Matsuda, Y. (2001). Physiological and Molecular Biological Characterization of Intracellular Carbonic Anhydrase from the Marine DiatomPhaeodactylum tricornutum. *Plant Physiology*, *126*(4), 1459–1470. http://doi.org/10.1104/pp.126.4.1459

Sunda, W. G., & Huntsman, S. A. (2005). Effect of CO2 supply and demand on zinc uptake and growth limitation in a coastal diatom. *Limnology and Oceanography*, *50*(4), 1181–1192.

Vardi, A., Thamatrakoln, K., Bidle, K. D., & Falkowski, P. G. (2008). Diatom genomes come of age. *Genome Biology*, *9*(12), 245.

Wingler, P. J. L. (2000). Photorespiration: metabolic pathways and their role in stress protection. *Philosophical Transactions of the Royal Society of London. Series B, Biological Sciences*, *355*(1402), 1517–29.

Xu, Y., Feng, L., Jeffrey, P. D., Shi, Y., & Morel, F. M. (2008). Structure and metal exchange in the cadmium carbonic anhydrase of marine diatoms. *Nature*, *452*(7183), 56–61.

Yee, D., & Morel, F. M. (1996). In vivo substitution of zinc by cobalt in carbonic anhydrase of a marine diatom. *Limnology and Oceanography*, *41*(3), 573–577.

Yool, A., & Tyrrell, T. (2003). Role of diatoms in regulating the ocean's silicon cycle. *Global Biogeochemical Cycles*, *17*(4).